Structural and Multidisciplinary Optimization (2020) 61:1515–1528
https://doi.org/10.1007/s00158-019-02432-2

RESEARCH PAPER

Toward the robust establishment of variable-fidelity surrogate models for hierarchical stiffened shells by two-step adaptive updating approach

Kuo Tian[1,2] · Zengcong Li[1] · Xiangtao Ma[1] · Haixin Zhao[1] · Jiaxin Zhang[3] · Bo Wang[1]

Received: 8 June 2019 / Revised: 14 August 2019 / Accepted: 14 October 2019 / Published online: 5 December 2019

Abstract

Since the high-fidelity model (HFM) of hierarchical stiffened shells is time-consuming, the sampling points based on HFM are generally few, which would result in a certain randomness of the sampling process. In some cases, the prediction accuracy of the variable-fidelity surrogate model (VFSM) is prone to be not robust and reliable. In order to improve the robustness of the prediction accuracy of VFSM, a two-step adaptive updating approach is proposed for the robust establishment of VFSM. In the first step, the leave-one-out (LOO) cross validation is carried out for sampling points of the low-fidelity model (LFM), aiming at finding out those with large prediction error. Then, these points are evaluated by HFM and then added into the original HFM set. In the second step, another LOO cross validation is performed on sampling points of the hybrid bridge function linking HFM and LFM. Based on the Voronoi diagram method, new updating points are chosen from where the largest prediction error of the bridge function lies, and then the VFSM is updated. After above two-step updating process, the VFSM is established. Three simple examples of test functions are firstly presented to verify the effectiveness and efficiency of the proposed method. Further, the proposed method is applied to an engineering example of hierarchical stiffened shells. In order to provide evaluation indexes for prediction accuracy and robustness of VFSM, the VFSM is established by multiple times, and the mean value and the standard deviation of the relative root mean square error (*RRMSE*) values of the multiple sets of VFSM are calculated. Results indicate that, under the similar computational cost, the mean value and the standard deviation of the *RRMSE* values of the proposed method decrease by 24.1% and 82.0% than those of the traditional VFSM based on the direct sampling method, respectively. Therefore, the high prediction accuracy and robustness of the proposed method is verified. Additionally, the total computational time of the proposed VFSM decreases by 70% than that of the surrogate model based on HFM when achieving the similar prediction accuracy, indicating the high prediction efficiency of the proposed VFSM.

Keywords Variable-fidelity surrogate models · Adaptive updating approach · Hierarchical stiffened shells · Shell buckling

Responsible Editor: Nam Ho Kim

Electronic supplementary material The online version of this article (https://doi.org/10.1007/s00158-019-02432-2) contains supplementary material, which is available to authorized users.

✉ Kuo Tian
tiankuo@dlut.edu.cn

[1] Department of Engineering Mechanics, State Key Laboratory of Structural Analysis for Industrial Equipment, Dalian University of Technology, Dalian 116024, China

[2] School of Mechanical Engineering, Dalian University of Technology, Dalian 116024, China

[3] Department of Civil Engineering, Johns Hopkins University, Baltimore, MD 21218, USA

1 Introduction

Stiffened shells have been widely used in fuel tanks and interstages of launch vehicles. Buckling is the major failure mode for stiffened shells under axial compression load. Aiming at improving the ability to resist buckling, hierarchical stiffened shells have been proposed as an innovative structural configuration of stiffened shells (Wang et al. 2014). Generally, the hierarchical stiffened shell is composed of the skin, major stiffeners, and minor stiffeners. In comparison to traditional stiffened shells, hierarchical stiffened shells have larger lightweight design space because the stiffeners are designed in multiple sizes (Hao et al. 2014). Based on the nonlinear FE analysis method, Tian et al. (Tian et al. 2018a) and Zhao et al. (Zhao et al. 2017) found the high load-

carrying ability of hierarchical stiffened shells. Wang et al. (Wang et al. 2014) and Sim et al. (Sim et al. 2018a), (Sim et al. 2018b) employed single perturbation load approach (SPLA) for the prediction of knockdown factors of hierarchical stiffened shells, and the conclusion was drawn that the hierarchical stiffened shell has lower imperfection sensitivity than the traditional stiffened shell. Above hierarchical stiffened shells are made of the aluminum alloy material. Recently, the carbon fiber-reinforced hierarchical stiffened shells were fabricated and tested (Jiang et al. 2017; Li et al. 2018; Wu et al. 2018). Experimental results indicated that the hierarchical stiffeners contribute to increasing the specific strength of composite hierarchical stiffened shells against failure. In order to achieve better mechanical properties, optimizations were carried out for hierarchical stiffened shells (Quinn et al. 2012; Wang et al. 2017a; Wang et al. 2015). Tian et al. (Tian et al. 2018a) pointed out that the optimization of hierarchical stiffened shells is so time-consuming that the global optimizing ability of the optimization is greatly challenged.

One way to increase the computational efficiency of optimizations of hierarchical stiffened shells is developing efficient analysis models for hierarchical stiffened shells. For instance, Sun et al. (Sun et al. 2013) and Xu et al. (Xu et al. 2016) derived analytical methods for stiffened panels. Liu et al. (Liu et al. 2018) proposed an efficient method based on the mechanics of structure genome (MSG) for the global buckling analysis of stiffened composite panels, which can predict buckling loads and buckling modes accurately. Based on asymptotic homogenization method (AHM) and Rayleigh-Ritz method, Wang et al. (Wang et al. 2017b) developed the numerical-based smeared stiffener method (NSSM) for the fast prediction of linear buckling loads of composite hierarchical stiffened shells. Considering the post-buckling behavior of hierarchical stiffened shells, Wang et al. (Wang et al. 2017a) proposed a hybrid equivalent model for hierarchical stiffened shells by smearing out the minor stiffeners using AHM. By applying proper orthogonal decomposition method into the eigenvalue buckling method, Tian et al. (Tian et al. 2018b) proposed a reduced order model for the linear buckling prediction of composite shells.

Another way to increase the computational efficiency of optimizations of hierarchical stiffened shells is establishing the surrogate models. Li et al. (Li et al. 2016), Chen et al. (Chen et al. 2018), and Keshtegar et al. (Keshtegar and Hao 2018) employed kriging surrogate models to optimize stiffened shells. An adaptive response surface method was proposed for the optimization of stiffened panels (Keshtegar et al. 2018). In order to improve the optimization efficiency of variable stiffness composite shells, RBF-based surrogate modeling technique was used in Refs. (Rouhi et al. 2016), (Ghayoor et al. 2017). With respect to hierarchical stiffened shells, Wang et al. (Wang et al. 2017a), Hao et al. (Hao et al. 2014), Tian et al. (Tian et al. 2018a), and Zhao et al. (Zhao et al. 2017) applied RBF surrogate models into post-buckling optimizations, which significantly reduced the total computational cost. Aiming at improving the global optimizing ability of surrogate-based optimizations of stiffened panels and shells, Chagraoui et al. (Chagraoui and Soula 2018) combined the collaborative optimization method with the artificial neural network (ANN) surrogate model, and Wang et al. (Wang et al. 2017b) integrated the fixed-point method with the RBF surrogate model. In order to accelerate the sampling process of surrogate models, improved sampling methods were presented by Shields and Zhang (Shields and Zhang 2016).

Although using surrogate models, the sampling process based on the high-fidelity model (HFM) is still time-consuming. In this case, the variable-fidelity surrogate model (VFSM) method was proposed by combining the HFM with the low-fidelity model (LFM) (Forrester et al. 2007). Compared with the traditional surrogate model, VFSM can achieve similar prediction accuracy but with less computational cost. The most popular method used for constructing VFSM is the bridge function, which can be multiplicative, additive, or hybrid multiplicative/additive (Han and Görtz 2012). Co-RBF and co-kriging methods were used for developing VFSM (Song et al. 2019), (Han et al. 2012). Han et al. (Han et al. 2013) improved VFSM by means of gradient-enhanced kriging and a generalized hybrid bridge function. Based on the active learning method, Zhou et al. (Zhou et al. 2016a), (Zhou et al. 2016b) proposed an efficient sequential sampling method, which significantly improved the prediction accuracy of VFSM. Giselle Fernández-Godino et al. (Giselle Fernández-Godino et al. 2019) pointed out that the inclusion of LFM in building VFSM led to less accurate VFSM than just using the available HFM in some cases. It means that the VFSM may be not robust or reliable due to the influence of LFM in some cases. In other words, LFM behaves like the "noise" to disturb the accurate establishment of VFSM. In order to guarantee the prediction accuracy and robustness of VFSM, it is meaningful to develop a robust establishment method for constructing VFSM, which is the objective of this paper.

The outline of this paper is organized as follows. In Sect. 2, the HFM and LFM of hierarchical stiffened shells are introduced briefly, and then the two-step adaptive updating approach is developed for the robust establishment of VFSM. In Sect. 3, three simple examples of test functions and an engineering example of hierarchical stiffened shells are used to validate the prediction accuracy and efficiency of the proposed VFSM in comparison to the traditional VFSM. The final part is the conclusion.

2 Two-step adaptive updating approach for the robust establishment of variable-fidelity surrogate models

2.1 HFM and LFM for hierarchical stiffened shells

In this paper, the FE model with full structural details is regarded as the HFM for hierarchical stiffened shells (as

shown in Fig.1 (b)), which is calculated based on the explicit dynamic method to capture the collapse load. The formula of the explicit dynamic method is expressed as

$$\mathbf{M}\mathbf{a}_t = \mathbf{F}_t^{ext} - \mathbf{F}_t^{int} - \mathbf{C}\mathbf{V}_t - \mathbf{K}\mathbf{U}_t \tag{1}$$

where, $\boldsymbol{M}$ is the mass matrix, $\boldsymbol{a}$ is the vector of nodal acceleration, $\mathbf{F}^{ext}$ is the vector of applied external force, $\mathbf{F}^{int}$ is the vector of internal force, $\boldsymbol{C}$ is the damping matrix, $\boldsymbol{V}$ is the vector of nodal velocity, $\boldsymbol{K}$ is the stiffness matrix, $\boldsymbol{U}$ is the vector of nodal displacement, and t is the time. In this paper, the explicit time integration with the central difference approach is used to approximate velocity and acceleration.

The HFM was validated to have good agreement with experimental results (Tian et al. 2018c), (Wang et al. 2019). However, the HFM is generally time-consuming due to the complex stiffeners of hierarchical stiffened shells, especially the minor stiffeners (Wang et al. 2017a). It can be expected that, if the minor stiffeners were smeared out, the computational cost of hierarchical stiffened shells would decrease significantly. In this paper, AHM is employed for the equivalence of minor stiffeners, and thus the LFM of hierarchical stiffened shells can be established, as shown in Fig.1 (c). A brief introduction of the procedure of AHM is as follows.

Step 1: A representative unit cell (RUC) is divided out of the stiffened shell, and its FE model is built. Then, the unit nodal displacement fields χ_i^0 and $\overline{\chi}_i^0$ are imposed on the RUC. Subscripts i and j denote load cases ($i, j \in \{1, 2, 6\}$). The variables with the overline stand for the flexural variables, and the others stand for in-plane variables. The first static analysis is performed on the RUC, and the nodal force vectors $\mathbf{f}_i$ and $\overline{\mathbf{f}}_i$ are outputted.

Step 2: The outputted force vectors are then applied to each node of the original RUC, and periodic boundary conditions are set up. Furthermore, the second static analysis is performed on the RUC, and characteristic nodal displacements $\mathbf{a}_i^*$ and $\overline{\mathbf{a}}_i^*$ are outputted.

Step 3: Above characteristic nodal displacement fields $\mathbf{a}_i^*$ and $\overline{\mathbf{a}}_i^*$ are applied to corresponding nodes of the original RUC, and then the third static analysis is carried out to calculate the characteristic nodal reaction forces $\mathbf{P}_i^*$ and $\overline{\mathbf{P}}_i^*$.

Step 4: The extensional stiffness coefficients $\boldsymbol{A}_{ij}$, coupling stiffness coefficients $\boldsymbol{B}_{ij}$, and bending stiffness coefficients $\boldsymbol{D}_{ij}$ of the RUC with the volume Ω can be obtained directly by the dot product operation of unit nodal displacement vectors, nodal force vectors, characteristic nodal displacements vectors, and characteristic nodal force vectors. The expression is as follows.

$$\begin{aligned} A_{ij} &= \frac{1}{|\Omega|}\left(\chi_i^0 - \mathbf{a}_i^*\right)^{\mathrm{T}}\left(\mathbf{f}_j - \mathbf{P}_j^*\right) \\ B_{ij} &= \frac{1}{|\Omega|}\left(\chi_i^0 - \mathbf{a}_i^*\right)^{\mathrm{T}}\left(\overline{\mathbf{f}}_j - \overline{\mathbf{P}}_j^*\right) \\ D_{ij} &= \frac{1}{|\Omega|}\left(\overline{\chi}_i^0 - \overline{\mathbf{a}}_i^*\right)^{\mathrm{T}}\left(\overline{\mathbf{f}}_j - \overline{\mathbf{P}}_j^*\right) \end{aligned} \tag{2}$$

By means of above steps, the minor stiffeners and skin of hierarchical stiffened shells can be together equivalent to an unstiffened panel with effective stiffness coefficients A_{ij}, B_{ij}, and D_{ij}, while keeping major stiffeners remained. Thus, the LFM of hierarchical stiffened shells is established, as shown in Fig.1 (c). More details about the LFM of hierarchical stiffened shells can refer to Ref. (Wang et al. 2017a).

2.2 Two-step adaptive updating approach for the robust establishment of VFSM

Due to the fact that the HFM of hierarchical stiffened shells is time-consuming, the sampling points based on HFM are generally few when building a VFSM, which would result in a certain randomness of the sampling process of HFM. In order to guarantee the prediction accuracy and robustness of VFSM, the first-step updating is carried out for HFM. Here, it is assumed that the changing tendency of the prediction accuracy between HFM and LFM is similar. Besides, LFM is supposed to have better ability to describe the design domain than HFM because the number of sampling points of LFM is larger than that of HFM. Thus, the main concept of the first-step updating is to use the cross validation result of LFM to find sampling points with large prediction errors and then guide the updating of sampling points of HFM, as shown in Fig.2 (b). After the first-step updating, VFSM can be established by combining

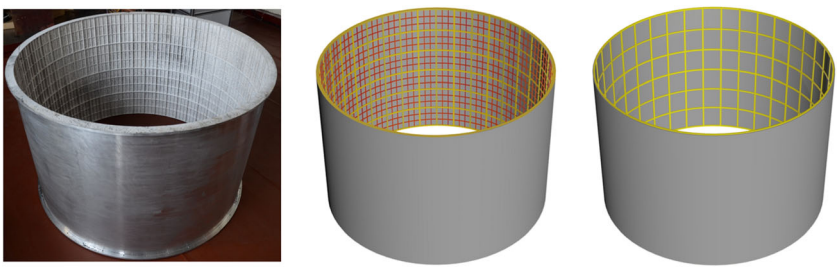

(a) Test model (b) High-fidelity FE model (c) Low-fidelity FE model

Fig. 1 Schematic diagram of hierarchical stiffened shell

HFM with LFM via the bridge function. However, there would be a certain randomness of the prediction accuracy of the bridge function when employing the direct establishment of the bridge function based on original sampling points of HFM and LFM. In some cases, it would construct a VFSM with the low prediction accuracy. Thus, the main concept of the second-step updating is to use the cross validation result of the bridge function to find sampling points with large prediction errors and then guide the updating of sampling points of the bridge function, as shown in Fig.2 (c). By means of the two-step updating approach, the updated VFSM can be obtained.

To sum up, the prediction accuracy of VFSM heavily depends on the sampling points, and the direct establishment method of VFSM based on original sampling points without updating would cause a certain randomness of the sampling process of HFM and bridge function, which would result in low prediction accuracy of VFSM. Thus, the main purpose of this paper is to develop a two-step adaptive updating approach for the robust establishment of VFSM.

The flow chart of the two-step adaptive updating approach for VFSM is displayed in Fig. 3.

Step 1: *M* and *N* sampling points are generated in the design space and then calculated based on HFM and LFM, respectively. For the example of hierarchical stiffened shells, the ratio between the single analysis time of HFM and LFM is about 19:1. Many examples with similar ratio were studied in Refs. (Tyan et al. 2015; Vitali et al. 2002; Molina-Cristóbal et al. 2010), and their ratios between *M* and *N* are 5.8%, 3.4%, and 6%, respectively. Besides, by trial and error of several test functions and engineering examples of hierarchical stiffened shells, the VFSM behaves best when *M* is less than 10% of *N*. Above all, *M* is suggested to be less than 10% of *N* for similar VFSM problems.

The leave-one-out (LOO) cross validation is performed on sampling points of the LFM, and sampling points are ranked from the largest to the smallest according to the relative error results. The first *n* sampling points with the largest prediction error are chosen and calculated based on the HFM. Then, they are added into the original HFM to generate the updated HFM.

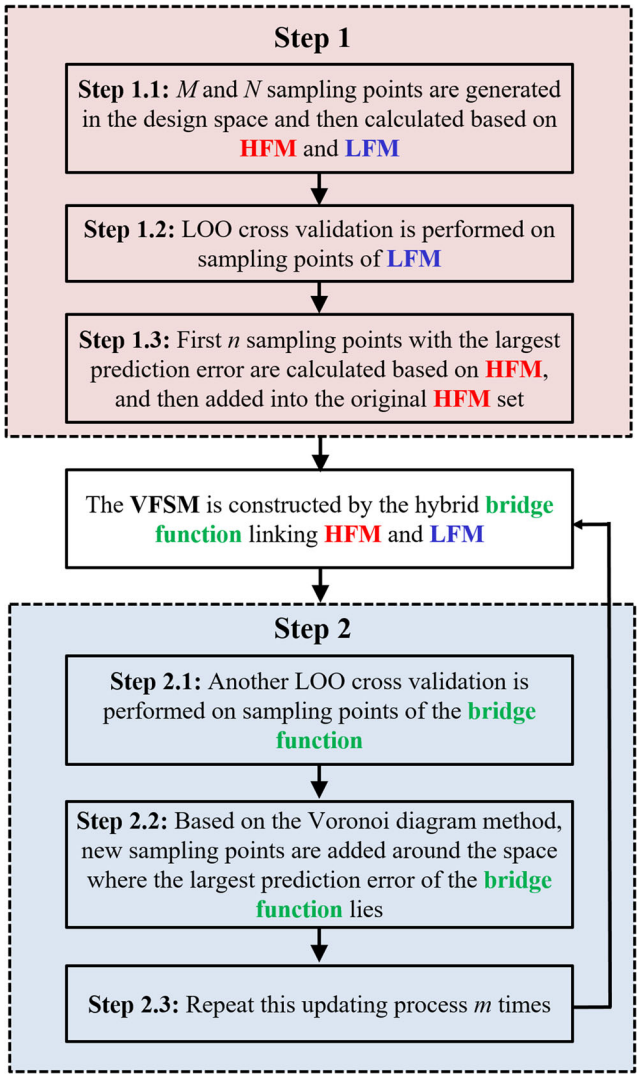

Fig. 3 Flow chart of the two-step adaptive updating approach for the robust establishment of VFSM

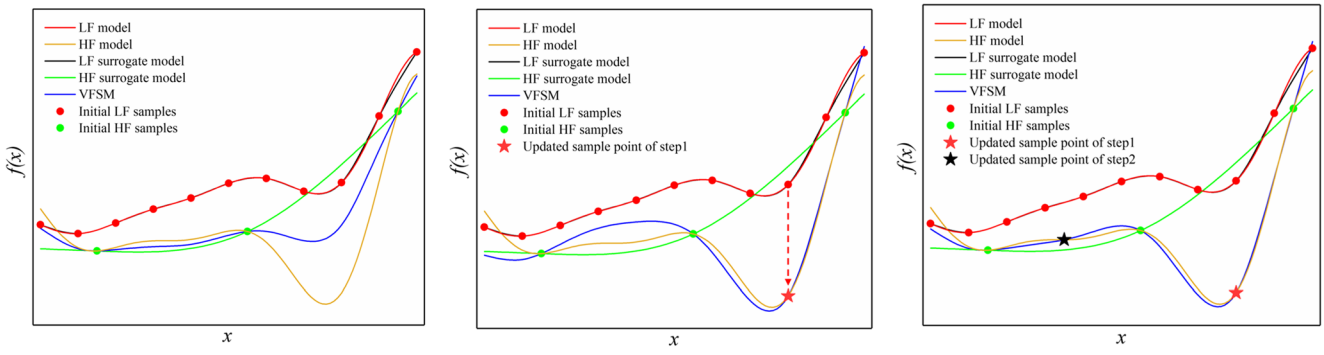

(a) Original VFSM (b) Updated VFSM in Step 1 (c) Updated VFSM in Step 2

Fig. 2 Illustration of the procedure for two-step adaptive updating approach

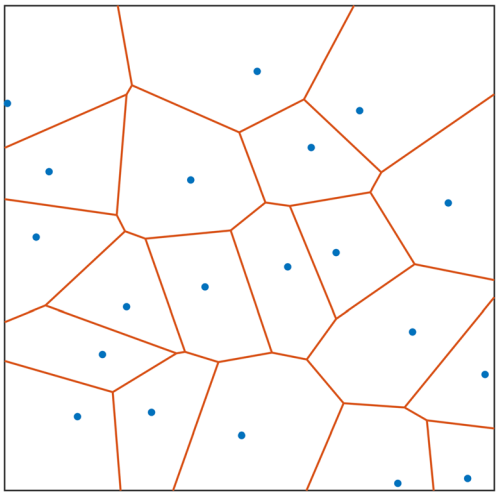

Fig. 4 Schematic diagram of Voronoi diagram method

By trial and error, the updating number n is suggested to be not larger than 50% of the initial number M of HFM.

Based on above sampling results, the VFSM is constructed via the bridge function. In this paper, the hybrid bridge function that combines the multiplicative and additive bridge functions is employed. As introduced in Ref. (Gano et al. 2004), its formula is as follows:

$$y_{VFSM} = \omega \cdot \rho(x) \cdot y_{LFM}(x) + (1-\omega)[y_{LFM}(x) + \delta(x)] \tag{3}$$

where y_{VFSM} is the VFSM, $y_{LFM}(x)$ is the LFM, and ω is the weight coefficient (ω= 0.5 in this paper). $\rho(x)$ and $\delta(x)$ are multiplicative and additive bridge functions, respectively, which can be regarded as the scaling ratio between HFM and LFM. They are expressed as

$$\rho(x) = \frac{y_{HFM}(x_{HFM})}{y_{LFM}(x_{HFM})} \tag{4}$$

$$\delta(x) = y_{HFM}(x_{HFM}) - y_{LFM}(x_{HFM}) \tag{5}$$

where y_{HFM} is the HFM and x_{HFM} is the set of sampling points based on HFM.

Step 2: Another LOO cross validation is performed on sampling points of the bridge function. Based on the Voronoi diagram method, new sampling points are added around the space where the largest prediction error of the bridge function lies. Repeat this updating process m times. According to Ref. (Aurenhammer 1991), the procedure of the Voronoi diagram method is summarized as follows.

First, the Voronoi diagram (Fig. 4) is used to partition the plane with k points ($S = \{x_1, x_2, \ldots, x_k\}$) into a set of Voronoi cells $C = \{C_1, C_2, \ldots, C_k\}$. For two distinct points $x_i, x_j \in S$, the dominance of x_i over x_j is defined as the subset of the plane being at least as close to x_i as to x_j, which is expressed as

$$dom(x_i, x_j) = \left\{ x \in R^n \middle| \|x - x_i\| \le \|x - x_j\| \right\} \tag{6}$$

where $dom(x_i, x_j)$ is a closed half plane bounded by the perpendicular bisector of x_i and x_j. The bisector separates all points of the plane closer to x_i from those closer to x_j. Then, the ith Voronoi cell C_i representing the surrounding region of point x_i can be determined as

$$C_i = \bigcap_{x_j \in S \setminus x_i} dom(x_i, x_j) \tag{7}$$

where C_i stands for the portion of the plane lying in all of the dominances of x_i over the remaining points in S. Since the Voronoi cell C_i is generated by intersecting k-1 half planes, it is a convex polygon. Thus, Voronoi cells form a polygonal partition of the plane, and this partition is called the Voronoi diagram.

Then, the LOO cross validation is carried out for k points in S. According to the LOO cross validation results, the point with the largest prediction error is selected, and the Voronoi cell corresponding to it is regarded as the sensitive Voronoi cell $C_{sensitive}$. A new point farthest away from the original point in $C_{sensitive}$ is chosen and determined as the updating point, which is then added into the original sampling points of the bridge function.

Table 1 Mean value, standard deviation and optimal value results for 25 sets of *RRMSE* and R^2 values of surrogate models of sinusoidal function

Surrogate model	Mean value		Standard deviation		Optimal value	
	RRMSE	R^2	*RRMSE*	R^2	*RRMSE*	R^2
25 HFM	0.809	0.317	0.102	0.172	0.626	0.594
300 LFM	0.462	0.782	0.012	0.0114	0.440	0.800
25 HFM + 300 LFM	0.476	0.766	0.064	0.0641	0.391	0.846
35 HFM + 300 LFM	0.371	0.857	0.046	0.0366	0.266	0.930
40 HFM + 300 LFM	0.339	0.879	0.057	0.0435	0.247	0.936
25 HFM + 300 LFM + 15 HFM (EI)	0.341	0.876	0.080	0.067	0.234	0.945
25 HFM + 300 LFM + 15 HFM (PoI)	0.356	0.867	0.058	0.044	0.252	0.933
25 HFM + 300 LFM + 10 HFM (Step1)	0.281	0.918	0.042	0.0246	0.180	0.966
25 HFM + 10 HFM (Step1)	0.551	0.671	0.133	0.170	0.348	0.880
300 LFM + 10 HFM (Step1)	0.736	0.445	0.090	0.134	0.578	0.665
25 HFM + 300 LFM + 10 HFM (Step1) + 5 HFM (Step2)	0.225	0.948	0.036	0.0156	0.145	0.978

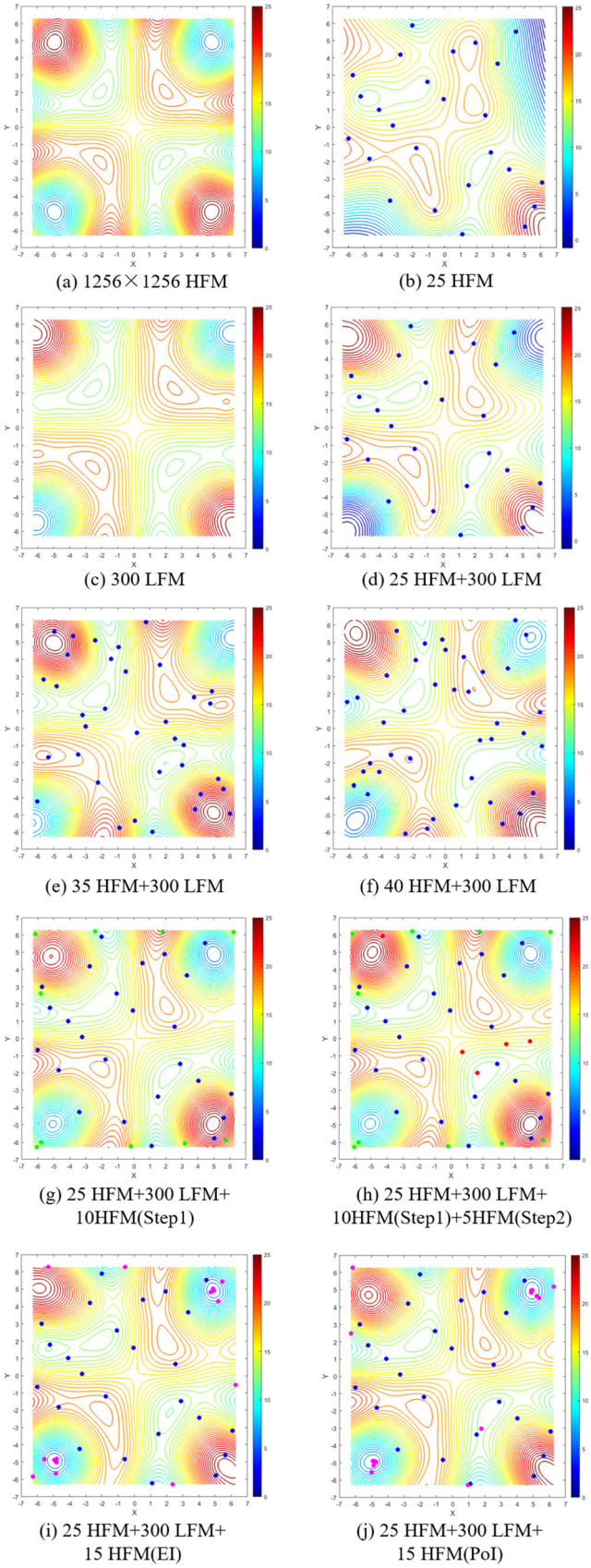

Fig. 5 Plots of surrogate models and sampling points of sinusoidal function

Based on above two-step adaptive updating approach, the VFSM can be established. In order to verify the prediction accuracy of the established VFSM, another set of sampling points is generated as the testing set and then calculated by HFM and VFSM, respectively. The prediction error of the testing set can be evaluated according to relative root mean square error (*RRMSE*) and R^2 values. The formulas are as follows:

$$RRMSE = \frac{\sqrt{\frac{1}{N}\sum_{i=1}^{K}\left(y_i - \hat{y}_i\right)^2}}{\sqrt{\frac{1}{N-1}\sum_{i=1}^{K}\left(y_i - \widetilde{y}_i\right)^2}} \tag{8}$$

$$R^2 = 1 - \frac{\sum_{i=1}^{K}\left(y_i - \hat{y}_i\right)^2}{\sum_{i=1}^{K}\left(y_i - \widetilde{y}_i\right)^2} \tag{9}$$

where K is the total number of sampling points of the testing set, y_i is the actual value of the ith sampling point by HFM, $\hat{y}_i$ is the predicted value by VFSM, and $\widetilde{y}_i$ is the mean value of the actual values of all sampling points by HFM. The more R^2 approximates to 1.0, the more accurate the VFSM is. The less *RRMSE* is, the more accurate the VFSM is.

3 Illustrative examples

3.1 Simple examples of test functions

Firstly, a sinusoidal function is taken as a simple example to verify the effectiveness of the proposed method, which is a common test function widely used for testing the variable-fidelity surrogate model and optimization algorithm (Zhou et al. 2016c), (Xu 2013). The formulas of the HFM and the LFM for the sinusoidal function are as follows:

$$f_h = x_1 \sin x_2 + x_2 \sin x_1 + 5\pi \tag{10}$$

$$f_l = 0.8x_1 \sin(0.9x_2) + 0.9x_2 \sin(0.8x_1) + 5\pi \tag{11}$$

where f_h represents the HFM and f_l represents the LFM, x_1, $x_2 \in [-2\pi, 2\pi]$.

Latin hypercube sampling (LHS) method is used to sample in the design space. Based on the sampling results, surrogate models of HFM, LFM, and VFSM are established, respectively. Another 200 sampling points are generated based on HFM as the testing set. Then, the prediction errors of surrogate models are evaluated by *RRMSE* and R^2 values. In order to study the robustness and reliability of surrogate models, sampling points are generated randomly by 25 times, and the mean value, standard deviation, and optimal value results of the 25 sets of *RRMSE* and R^2 values of surrogate models are calculated. The corresponding results are listed in Table 1. In

Table 2 Mean value, standard deviation and optimal value results for 25 sets of *RRMSE* and R^2 values of surrogate models of six-hump camelback function

Surrogate model	Mean value		Standard deviation		Optimal value	
	RRMSE	R^2	*RRMSE*	R^2	*RRMSE*	R^2
15 HFM	0.496	0.742	0.095	0.101	0.366	0.864
200 LFM	1.174	−0.394	0.004	0.015	1.164	−0.370
15 HFM + 200 LFM	0.440	0.797	0.086	0.083	0.323	0.893
20 HFM + 200 LFM	0.339	0.875	0.088	0.074	0.223	0.950
25 HFM + 200 LFM	0.259	0.930	0.050	0.028	0.184	0.966
15 HFM + 200 LFM + 5 HFM (Step1)	0.275	0.922	0.046	0.026	0.205	0.957
15 HFM + 5 HFM (Step1)	0.324	0.890	0.056	0.037	0.232	0.945
200 LFM + 5 HFM (Step1)	0.833	0.287	0.112	0.179	0.617	0.616
15 HFM + 200 LFM + 5 HFM (Step1) + 5 HFM (Step2)	0.215	0.953	0.028	0.012	0.155	0.976

order to determine whether the prediction accuracy of the surrogate model is high enough, a criterion is defined in this paper. When the mean value of the *RRMSE* value of the surrogate model is smaller than 0.230, the prediction accuracy of the surrogate model is considered to be high enough. From the *RRMSE* and R^2 values, it can be found that the prediction accuracy of the 25 HFM is the poorest. As for the 300 LFM, the prediction accuracy is higher than the 25 HFM; however, its prediction accuracy is still not high enough according to the criterion. By combining 25 HFM with 300 LFM, the VFSM is established. As the number of the HFM in the VFSM increases, the prediction error of the VFSM decreases gradually. For comparison, the proposed two-step adaptive updating approach is employed for the VFSM composed of 25 HFM and 300 LFM. In Step 1, ten sampling points are updated into the original VFSM. The prediction accuracy of the VFSM (25 HFM + 300 LFM + 10 HFM (Step1)) is listed in Table 1, which is higher than that of the VFSM (25 HFM + 300 LFM) without updating. In order to compare with the single-fidelity surrogate model, the surrogate model (25 HFM + 10 HFM (Step1)) and the surrogate model (300 LFM + 10 HFM (Step1)) are calculated, with results listed in Table 1. It can be found that the VFSM (25 HFM + 300 LFM + 10 HFM (Step1)) has higher prediction accuracy than these two single-fidelity surrogate models, which demonstrates the advantage of the updated VFSM in improving the prediction accuracy compared with the single-fidelity surrogate model.

In Step 2 of the proposed method, five sampling points are chosen and added into the VFSM according to the LOO cross validation result. In this case, the updated VFSM includes 25 HFM, 300 LFM, 10 HFM (Step1), and 5 HFM (Step2), which shares similar total computational cost with VFSM (40 HFM + 300 LFM). Compared with the results of VFSM (40 HFM + 300 LFM), the mean value, standard deviation, and optimal value of *RRMSE* values of updated VFSM (25 HFM + 300 LFM + 10 HFM (Step1) + 5 HFM (Step2)) reduce by 33.8%, 36.9%, and 41.4%, respectively, indicating high prediction accuracy of the proposed method. By comparing the standard deviation results, we can find out that the updated VFSM provides more robust and reliable prediction results than the traditional VFSM. It can be observed from Table 1 that the mean value, standard deviation, and optimal value of R^2 values have the similar trend as those of *RRMSE* values. For the sake of succinct statement, we take the results of *RRMSE* values into the primary consideration, and the results of R^2 values are regarded as a reference.

In particular, the proposed two-step adaptive updating approach is compared with other updating criterions, including expected improvement (EI) and probability of improvement (PoI). The detailed formulas and procedures of EI and PoI methods can refer to Refs. (Jones et al. 1998), (Viana and Haftka 2010). The prediction results of VFSMs by the two-step adaptive updating approach, the EI method, and the PoI method are evaluated and listed in Table 1. As for the

Table 3 Mean value, standard deviation, and optimal value results for 25 sets of *RRMSE* and R^2 values of surrogate models of Colville function

Surrogate model	Mean value		Standard deviation		Optimal value	
	RRMSE	R^2	*RRMSE*	R^2	*RRMSE*	R^2
15 HFM	0.580	0.630	0.155	0.201	0.306	0.902
200 LFM	0.842	0.274	0.018	0.030	0.801	0.339
15 HFM + 200 LFM	0.436	0.789	0.123	0.122	0.239	0.945
20 HFM + 200 LFM	0.362	0.862	0.076	0.058	0.234	0.942
25 HFM + 200 LFM	0.282	0.917	0.051	0.031	0.197	0.959
15 HFM + 200 LFM + 5 HFM (Step1)	0.305	0.901	0.055	0.037	0.232	0.948
15 HFM + 5 HFM (Step1)	0.786	0.365	0.104	0.157	0.550	0.682
200 LFM + 5 HFM (Step1)	1.343	−1.131	0.531	1.974	0.750	0.462
15 HFM + 200 LFM + 5 HFM (Step1) + 5 HFM (Step2)	0.238	0.942	0.021	0.010	0.194	0.963

Table 4 The design space for hierarchical stiffened shells

	t_s [mm]	t_{rj} [mm]	t_{rn} [mm]	h_{rj} [mm]	h_{rn} [mm]	N_{cj}	N_{cn}	N_{aj}	N_{an}
Lower bound	2.5	3.0	3.0	15.0	6.0	3	1	20	1
Upper bound	5.5	12.0	12.0	30.0	15.0	9	4	50	4

proposed two-step adaptive updating approach, the maximum number of updating points is 15. For a fair comparison, the maximum number of updating points for EI and PoI methods is also chosen as 15. It can be found that, under the similar computational cost, the prediction accuracy of the proposed method is significantly higher than EI and PoI methods, indicating the advantage of the proposed method in improving the prediction accuracy and robustness of VFSM.

A total of 1256 × 1256 sampling points are uniformly generated in the design space and evaluated by HFM, and then the sinusoidal function is plotted in Fig. 5 (a), which is regarded as the benchmark result. Above 1256 × 1256 sampling points are also evaluated by surrogate models of the 25 HFM, the 300 LHM, the VFSM (25 HFM + 300 LFM), the VFSM (35 HFM + 300 LFM), and the VFSM (40 HFM + 300 LFM), respectively. Their contour maps are plotted in Fig. 5 (b)–(f), and the original sampling points of HFM in VFSM are marked in blue. It can be observed that the 25 HFM has the largest prediction error. Although the VFSM would be more approximate to the benchmark result as the number of HFM in VFSM increases, the VFSM (40 HFM + 300 LFM) is still not able to describe the sinusoidal function accurately, especially for the region near the global optimum and the local optimum. The contour maps plotted by the VFSM (25 HFM + 300 LFM + 10 HFM(Step1)) and the VFSM (25 HFM + 300 LFM + 10 HFM(Step1) + 5 HFM(Step2)) are shown in Fig. 5 (g)–(h). The HFM sampling points generated by the Step 1 and the Step 2 updating processes are marked in green and red, respectively. It can be found that, after the updating of the Step 1 and the Step 2, sampling points are distributed adaptively

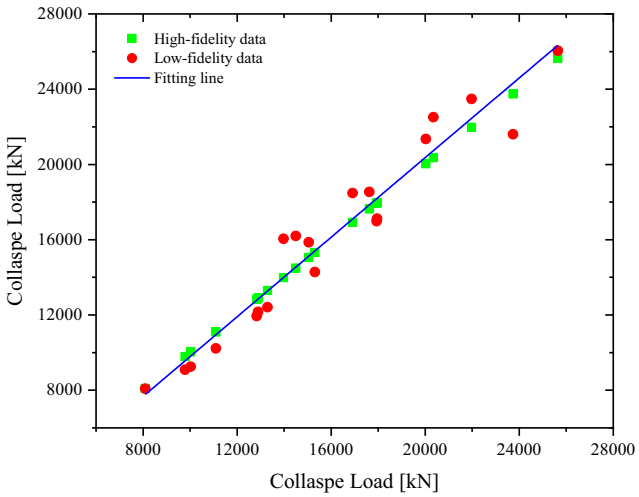

Fig. 6 Correlation analysis result between HFM and LFM

where the prediction error is large. Compared with the VFSM (40 HFM + 300 LFM), the VFSM (25 HFM + 300 LFM + 10 HFM(Step1) + 5 HFM(Step2)) is more approximate to the benchmark result, demonstrating the high prediction accuracy of the proposed method. Additionally, the contour maps plotted by the VFSM (25 HFM + 300 LFM + 15 HFM(EI)) and the VFSM (25 HFM + 300 LFM + 15 HFM(PoI)) are shown in Fig. 5 (i)–(j), and the updating points are marked in purple. It can be observed that these updating points tend to distribute locally around the global optimum, while the global prediction accuracy is not able to be guaranteed. Through the comprehensive comparison, the effectiveness of the proposed two-step adaptive updating approach is verified in this example.

Furthermore, another two test functions are carried out to verify the effectiveness of the proposed VFSM, including the six-hump camelback function (Ariyarit et al. 2018), (Molga and Smutnicki 2005) and the Colville function (Choi 2002), (Pires et al. 2010). As for the six-hump camelback function, the formulas of HFM and LFM are defined as

$$f(x_1,x_2) = 4x_1^2 - 2.1x_1^4 + x_1^6/3 + x_1x_2 - 4x_2^2 + 4x_2^4 \tag{12}$$

$$f_h = f(x_1,x_2) \tag{13}$$

$$f_l = f(0.6x_1,0.6x_2) + x_1x_2 + \sin(x_1) + \sin(x_2) + 2x_2 + x_1 \tag{14}$$

where x_1, $x_2 \in [-2, 2]$.

Similarly with the example of the sinusoidal function, the mean value, standard deviation, and optimal value results of the 25 sets of *RRMSE* and R^2 values of surrogate models are calculated to compare the proposed VFSM with the traditional VFSM, as listed in Table 2. When using the similar computational cost, the mean value, standard deviation, and optimal value of *RRMSE* values of updated VFSM (15 HFM + 200 LFM + 5 HFM (Step1) + 5 HFM (Step2)) reduce by 17.1%, 44.9%, and 16.2% than results of VFSM (25 HFM + 200 LFM), respectively. Thus, the high prediction accuracy and robustness of the proposed method is demonstrated.

With respect to the Colville function, the formulas of HFM and LFM are as follows:

$$\begin{aligned} f(x_1,x_2,x_3,x_4) = {} & 100\left(x_1^2 - x_2\right)^2 + (x_1-1)^2 \\ & + (x_3-1)^2 + 90\left(x_3^2 - x_4\right)^2 + 10.1\left((x_2-1)^2 + (x_4-1)^2\right) \\ & + 19.8(x_2-1)(x_4-1) \end{aligned} \tag{15}$$

$$f_h = f(x_1,x_2,x_3,x_4) \tag{16}$$

$$f_l = f(0.8x_1,0.8x_2,0.5x_3,0.5x_4) \tag{17}$$

where x_1, x_2, x_3, $x_4 \in [0, 1]$.

Table 5 RRMSE and R^2 values of HFM of hierarchical stiffened shells

	10 HFM	15 HFM	20 HFM	30 HFM	40 HFM	60 HFM	80 HFM	100 HFM
RRMSE	0.515	0.396	0.335	0.302	0.274	0.247	0.220	0.227
R^2	0.733	0.842	0.887	0.909	0.925	0.936	0.951	0.948

As shown in Table 3, the mean value, standard deviation, and optimal value results of the 25 sets of *RRMSE* and R^2 values of HFM, LFM, and VFSM with different numbers of sampling points are calculated. It can be observed that, under the similar computational cost, the mean value, standard deviation, and optimal value of *RRMSE* values of the updated VFSM (15 HFM + 200 LFM + 5 HFM (Step1) + 5 HFM (Step2)) reduce by 15.4%, 59.5%, and 1.5% than results of the VFSM (25 HFM + 200 LFM), respectively. The advantage of the proposed VFSM in improving the prediction accuracy and robustness is thus verified.

Above all, the effectiveness of the proposed VFSM has been fully verified through three illustrative examples of test functions.

3.2 Engineering example of hierarchical stiffened shells

Further, an engineering example of the hierarchical stiffened shell is studied. Its structural configuration is displayed in Fig. 1. The hierarchical stiffened shell has a diameter D of 3000 mm and a length L of 2000 mm. The hierarchical stiffened shell is composed of the skin, major stiffeners, and minor stiffeners. Here, t_s represents the skin thickness, N_{aj} represents the number of axial major stiffeners, N_{an} represents the axial minor stiffeners between axial major stiffeners, N_{cj} represents the number of circumferential major stiffeners, N_{cn} represents the circumferential minor stiffeners between circumferential major stiffeners, h_{rj} and h_{rn} represent the major and minor stiffener heights respectively, and t_{rj} and t_{rn} represent the major and minor stiffener thicknesses. The design space of above design variables are listed in Table 4. The mechanical properties of the hierarchical stiffened shell are as follows: Young's modulus E = 70.0 GPa and Poisson's ratio υ = 0.33. The boundary condition of the hierarchical stiffened shell is to keep the lower end of the hierarchical stiffened shell clamped and the upper end fixed except the degrees of freedom along the axial direction. A uniform axial load is applied to the upper end of the hierarchical stiffened shell. A workstation with the CPU of Intel Xeon E5-2687w @ 3.10GHz and 64G RAM is used.

Before establishing the VFSM, it is meaningful to observe the correlation relationship between HFM and LFM of hierarchical stiffened shells. Twenty sampling points are generated in the design space. HFM and LFM are employed to evaluate each sampling point, and the correlation analysis is carried out between HFM and LFM results. As displayed in Fig. 6, the correlation coefficient between HFM and LFM is 0.97, which indicates that the variation tendency of LFM has a good consistency with that of HFM. The HFM and the LFM are validated to have a strong correlation relationship. For single calculation, HFM and LFM of hierarchical stiffened shells need about 1.5 h and 0.08 h, respectively. In other word, the computational time of 19 LFM equals to that of 1 HFM.

Next, the prediction accuracy of the surrogate model based on HFM is investigated. The number of HFM sampling points used for training varies from 10 to 100, as shown in Table 5. Then, another 200 sampling points are generated based on HFM as the testing set. The prediction results of surrogate models based on HFM are listed in Table 5 and Fig. 7. It can be found that, as the number of HFM increases, the *RRMSE* value decreases gradually until it reaches 80 HFM; however,

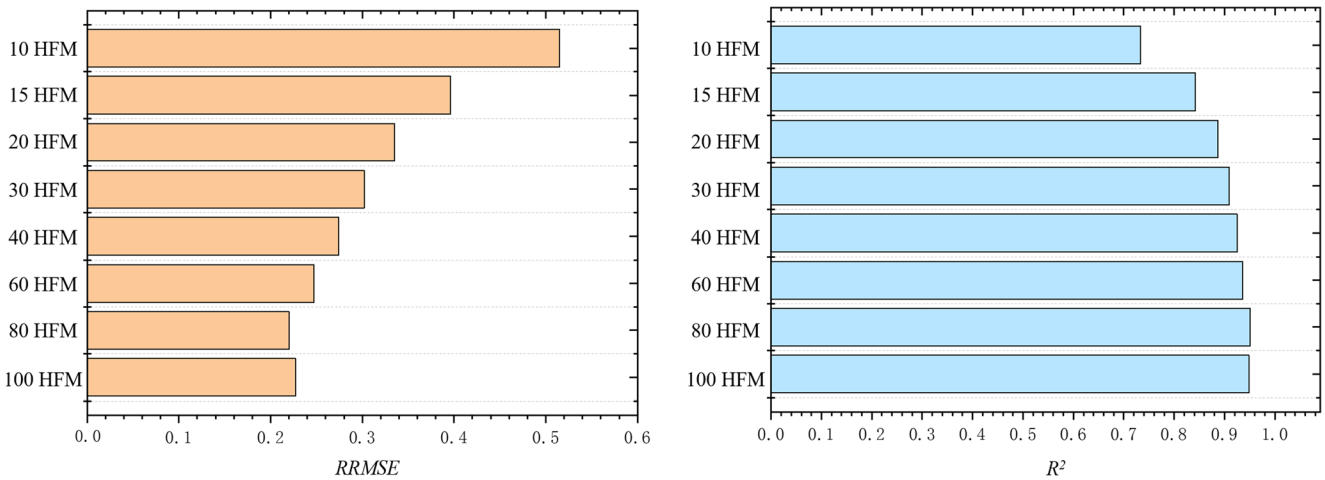

Fig. 7 Comparison of *RRMSE* and R^2 values of HFM of hierarchical stiffened shells

Table 6 *RRMSE* and R^2 values of LFM of hierarchical stiffened shells

	100 LFM	150 LFM	200 LFM	300 LFM	1000 LFM
RRMSE	0.383	0.327	0.340	0.338	0.325
R^2	0.853	0.893	0.884	0.885	0.894

the *RRMSE* value of 100 HFM is slightly lower than that of 80 HFM. In order to find out the reason, new sets of 80 HFM and 100 HFM are generated by LHS and their *RRMSE* values are 0.232 and 0.216, respectively. In this case, the *RRMSE* value of 100 HFM is higher than that of 80 HFM. This conclusion is opposite to that of previous sets of 80 HFM and 100 HFM. It can be inferred that, since the design space is large and the number of HFM sampling points is few, it would result in a certain randomness of the prediction accuracy of the sampling result. This randomness is supposed to be the main reason that the *RRMSE* value of 100 HFM is slightly lower than that of 80 HFM as shown in Table 5. Fortunately, the purpose of this paper is to reduce the randomness of the sampling process based on HFM. Along with the increase of the prediction accuracy, the total computational cost increases sharply, and it needs about 170 h to obtain 100 HFM, which is too time-consuming. By contrast, the prediction accuracy of the surrogate model based on the LFM is investigated, as shown in Table 6 and Fig. 8. As the number of LFM increases, the *RRMSE* value decreases gradually to 0.325 when it reaches 1000 LFM. It can be inferred that, even though further increasing the number of LFM, the prediction error would not increase significantly.

By combining 10 HFM with 200 LFM, the VFSM is established. In order to investigate the robustness and reliability of the VFSM, 10 HFM sampling points are generated randomly by 15 times, and the mean value, standard deviation, and optimal value results of the 15 sets of *RRMSE* and R^2 values of VFSM are calculated, as shown in Table 7, Fig. 9, Fig. 10, and Fig. 11. The optimal value of the *RRMSE* value of VFSM (10 HFM + 200 LFM) is 0.319, which is smaller than that of 10 HFM (0.515) and that of 200 LFM (0.340), indicating that the VFSM is effective in this case. However, the mean value of the *RRMSE* value of VFSM (10 HFM + 200 LFM) is 0.548, which means that the mean level of VFSM (10 HFM + 200 LFM) has larger prediction error than those of 10 HFM and 200 LFM, and thus the VFSM (10 HFM + 200 LFM) is verified to be not effective in most cases. The standard deviation of the *RRMSE* value of VFSM (10 HFM + 200 LFM) is quite large, which demonstrates that the traditional establishment of VFSM is not robust in some cases.

With respect to the VFSM (10 HFM + 200 LFM), the proposed two-step adaptive updating approach is applied. The updating numbers of sampling points are both set as 5 for Step 1 and Step 2. After the adaptive updating approach of Step 1 and Step 2, the prediction error results are listed in Table 7, Fig. 9, Fig. 10, and Fig. 11. In this VFSM (10 HFM + 200 LFM + 5 HFM (Step1) + 5 HFM (Step2)), the total computational cost is equal to that of the VFSM (20 HFM + 200 LFM). By comparing the mean value of the *RRMSE* values, it is found that the VFSM (10 HFM + 200 LFM + 5 HFM (Step1) + 5 HFM (Step2)) decreases by 24.1% than the VFSM (20 HFM + 200 LFM), indicating low average prediction error of the proposed method. The standard deviation of the *RRMSE* values of the VFSM (10 HFM + 200 LFM + 5 HFM (Step1) + 5 HFM (Step2)) decreases by 82.0% than that of the VFSM (20 HFM + 200 LFM), which demonstrates that the proposed method can provide more robust prediction results than the traditional VFSM. As for the mean value and the standard deviation results of the R^2 value, similar conclusions

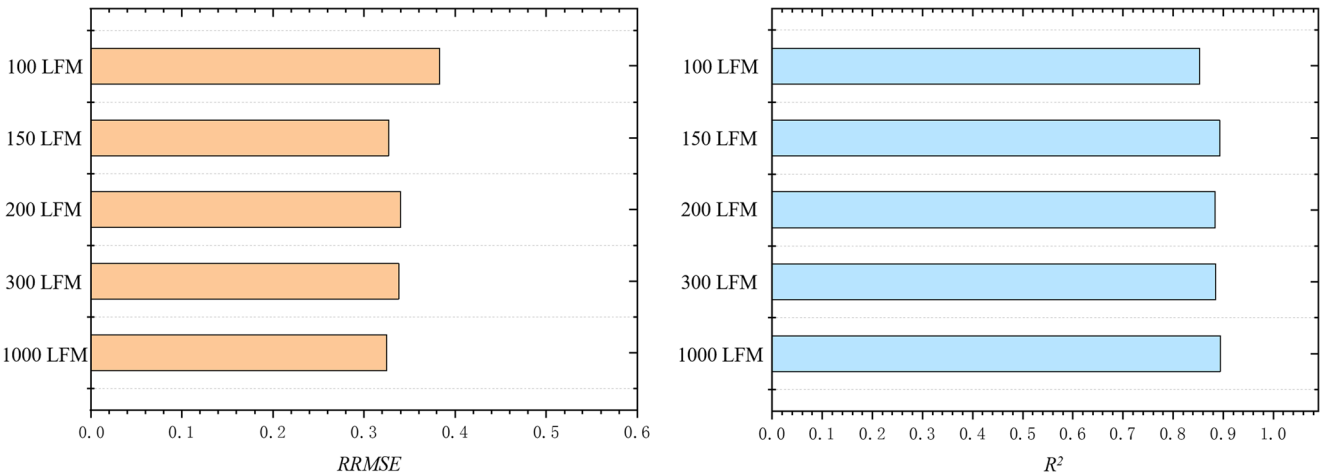

Fig. 8 Comparison of *RRMSE* and R^2 values of LFM of hierarchical stiffened shells

Table 7 Mean value, standard deviation, and optimal value results for 15 sets of *RRMSE* and R^2 values of VFSM of hierarchical stiffened shells

Surrogate model	Mean value		Standard deviation		Optimal value	
	RRMSE	R^2	*RRMSE*	R^2	*RRMSE*	R^2
10 HFM + 200 LFM	0.548	0.671	0.164	0.192	0.319	0.898
20 HFM + 200 LFM	0.312	0.899	0.057	0.0399	0.236	0.944
10 HFM + 200 LFM + 5 HFM (Step1)	0.267	0.926	0.027	0.0155	0.227	0.948
10 HFM + 200 LFM + 5 HFM (Step1) + 5 HFM (Step2)	0.237	0.943	0.010	0.005	0.220	0.951
15 HFM + 150 LFM + 5 HFM (Step1) + 5 HFM (Step2)	0.255	0.935	0.023	0.011	0.222	0.950

can be found as those of the *RRMSE* value. After comparing the prediction accuracy of HFM in Table 5 and VFSM in Table 6, it can be found that the VFSM (10 HFM + 200 LFM + 5 HFM (Step1) + 5 HFM (Step2)) has the similar prediction accuracy as the surrogate model based on 100 HFM; however, the total computational time of the VFSM (10 HFM + 200 LFM + 5 HFM (Step1) + 5 HFM (Step2)) decreases by 70% than that of the surrogate model based on 100 HFM, indicating the high prediction efficiency of the proposed VFSM. Above all, it can be concluded that the proposed two-step adaptive updating approach contributes to reducing the instability of the prediction accuracy of the traditional VFSM caused by the randomness of original sampling points and then guaranteeing the prediction accuracy of VFSM in a relatively high level.

It should be noted that the proposed establishment method of VFSM does not aim at the specific number of LFM or HFM, so it can be used for different combinations of LFM and HFM with different numbers of sampling points. The purpose of this paper is to provide a general framework to establish robust VFSM. In order to verify this point, another VFSM with a different combination of LFM and HFM is generated for comparison, including 15 HFM and 150 LFM. Following the proposed two-step adaptive updating approach, five sampling points are updated in Step 1 and Step 2, respectively, which is identical with the VFSM (10 HFM + 200 LFM + 5 HFM (Step1) + 5 HFM (Step2)). For the VFSM (15 HFM + 150 LFM + 5 HFM (Step1) + 5 HFM (Step2)), the mean value, standard deviation, and optimal value of *RRMSE* and R^2 values are listed in Table 7. It can be found that the VFSM (15 HFM + 150 LFM + 5 HFM (Step1) + 5 HFM (Step2)) and the VFSM (10 HFM + 200 LFM + 5 HFM (Step1) + 5 HFM (Step2)) both achieve relatively high prediction accuracy in comparison to the traditional VFSM, such as the VFSM (20 HFM + 200 LFM). It indicates that the proposed method can be used for different combinations of LFM and HFM with different numbers of sampling points.

4 Conclusions

In order to improve the robustness and reliability of VFSM, a novel establishment method of VFSM based on the two-step adaptive updating approach is proposed in this paper. The key

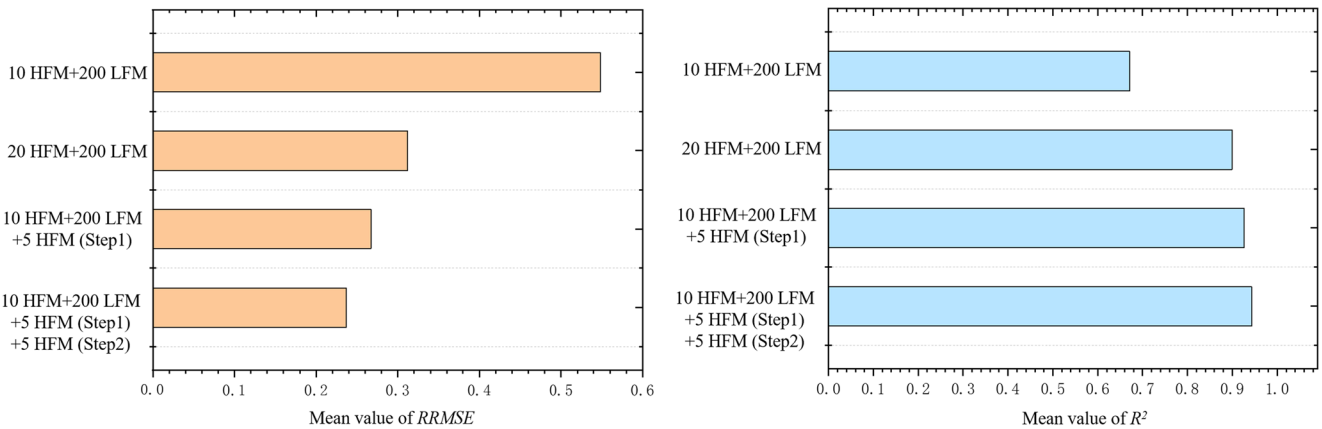

Fig. 9 Comparison of mean value of *RRMSE* and R^2 values of VFSM of hierarchical stiffened shells

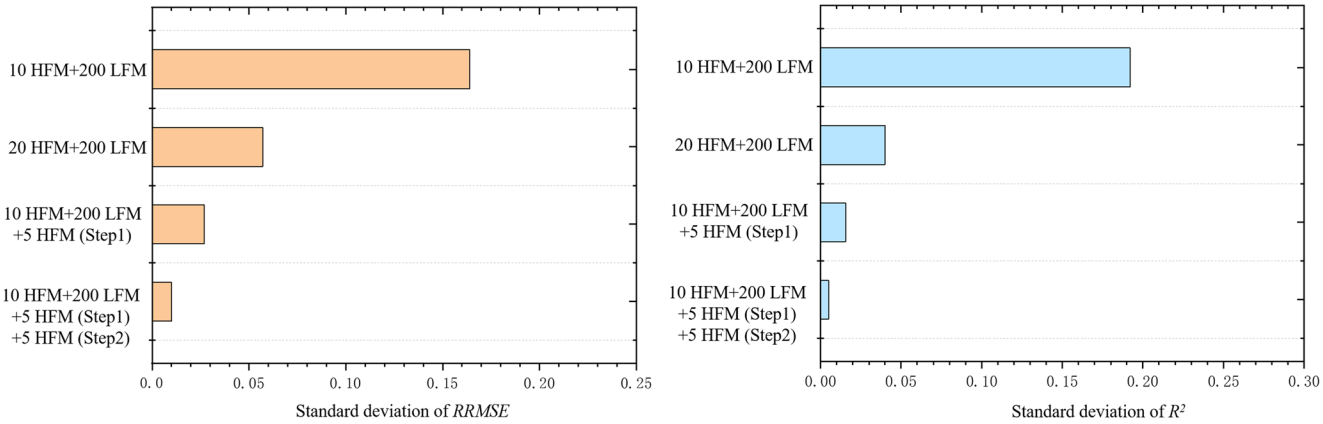

Fig. 10 Comparison of standard deviation of *RRMSE* and R^2 values of VFSM of hierarchical stiffened shells

part of the proposed method is as follows. In the first step, the LOO cross validation is carried out for sampling points of LFM, to find out those with large prediction error. After that, these new sampling points are evaluated by HFM and then added into the original HFM set. In the second step, another LOO cross validation is performed on sampling points of the bridge function. By means of the Voronoi diagram method, new points are chosen from where the largest prediction error of the bridge function lies. Then, these points are calculated by HFM and added into the VFSM to obtain the updated VFSM. Three simple examples of test functions are firstly presented to verify the effectiveness and efficiency of the proposed method. Moreover, an engineering example of hierarchical stiffened shells is carried out. In comparison to the traditional VFSM, the mean value and standard deviation of *RRMSE* values of the updated VFSM decrease by 24.1% and 82.0%, respectively. When achieving the similar prediction accuracy, the total computational time of the proposed method decreases by 70% than that of the surrogate model based on HFM, indicating the high prediction efficiency of the proposed method. Through these examples, the high prediction accuracy and robustness of the proposed method is fully verified. In the future study, optimizations based on the proposed VFSM will be carried out, and the effectiveness and efficiency of the optimization framework will be investigated.

5 Replication of results

The algorithm of the two-step adaptive updating approach is written in Matlab, and the FE model of the hierarchical stiffened shell is established in Python script, which are protected intellectual properties of Dalian University of Technology. And now we are applying for the software copyright. Thus, we are not allowed to provide all the code at present. If you are interested in it, you can get part of the code through emailing the corresponding author. In order to make the replication of results easier, the data points are provided as the supplementary material.

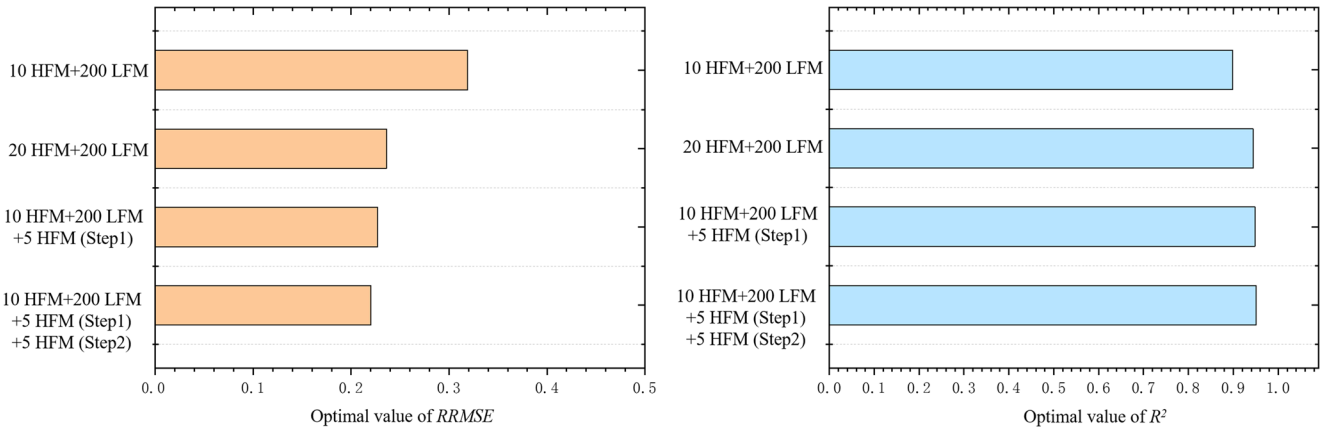

Fig. 11 Comparison of optimal value of *RRMSE* and R^2 values of VFSM of hierarchical stiffened shells.

Funding information This work was supported by China Postdoctoral Science Foundation [No. 2019 M651107], National Natural Science Foundation of China [No.1190020911, No.11825202], and LiaoNing Revitalization Talents Program [No. XLYC1802020]. Particularly, we gratefully acknowledge the helpful suggestions of Dr. Yan Zhou from Dalian University of Technology.

Compliance with ethical standards

Conflict of interest The authors declare that they have no conflict of interest.

References

Ariyarit A, Sugiura M, Tanabe Y et al (2018) Hybrid surrogate-model-based multi-fidelity efficient global optimization applied to helicopter blade design. Eng Optim 50(6):1016–1040

Aurenhammer F (1991) Voronoi diagrams-a survey of a fundamental geometric data structure. ACM Comput Surv (CSUR) 23(3):345–405

Chagraoui H, Soula M (2018) Multidisciplinary design optimization of stiffened panels using collaborative optimization and artificial neural network. Proc Inst Mech Eng Part C J Mech Eng Sci 232(20):3595–3611

Chen HS, Meng Z, Zhou HL (2018) A hybrid framework of efficient multi-objective optimization of stiffened shells with imperfection. Int J Comput Methods 15(8):1850145

Choi DH (2002) Cooperative mutation based evolutionary programming for continuous function optimization. Oper Res Lett 30(3):195–201

Forrester AIJ, Sóbester A, Keane AJ (2007) Multi-fidelity optimization via surrogate modelling. Proc Royal Soc A Math Phys Eng Sci 463(2088):3251–3269

Gano S, Sanders B, Renaud J 2004. Variable fidelity optimization using a kriging based scaling function. 10th AIAA/ISSMO Multidisciplinary Analysis and Optimization Conference: 4460.

Ghayoor H, Rouhi M, Hoa SV et al (2017) Use of curvilinear fibers for improved bending-induced buckling capacity of elliptical composite cylinders. Int J Solids Struct 109:112–122

Giselle Fernández-Godino M, Park C, Kim N H, et al. 2019 Issues in deciding whether to use multifidelity surrogates. AIAA J: 1-16.

Han ZH, Görtz S (2012) Hierarchical kriging model for variable-fidelity surrogate modeling. AIAA J 50(9):1885–1896

Han Z, Zimmerman R, Görtz S (2012) Alternative cokriging method for variable-fidelity surrogate modeling. AIAA J 50(5):1205–1210

Han ZH, Görtz S, Zimmermann R (2013) Improving variable-fidelity surrogate modeling via gradient-enhanced kriging and a generalized hybrid bridge function. Aerosp Sci Technol 25(1):177–189

Hao P, Wang B, Li G et al (2014) Hybrid optimization of hierarchical stiffened shells based on smeared stiffener method and finite element method. Thin-Walled Struct 82:46–54

Jiang S, Sun FF, Fan HL et al (2017) Fabrication and testing of composite orthogrid sandwich cylinder. Compos Sci Technol 142:171–179

Jones DR, Schonlau M, Welch WJ (1998) Efficient global optimization of expensive black-box functions. J Global Optim 13(4):455–492

Keshtegar B, Hao P (2018) A hybrid descent mean value for accurate and efficient performance measure approach of reliability-based design optimization. Comput Methods Appl Mech Eng 336:237–259

Keshtegar B, Hao P, Wang YT et al (2018) An adaptive response surface method and Gaussian global-best harmony search algorithm for optimization of aircraft stiffened panels. Appl Soft Comput 66:196–207

Li G, Meng Z, Hao P et al (2016) A hybrid reliability-based design optimization approach with adaptive chaos control using kriging model. Int J Comput Methods 13(1):1650006

Li M, Sun FF, Lai CL et al (2018) Fabrication and testing of composite hierarchical isogrid stiffened cylinder. Compos Sci Technol 157: 152–159

Liu N, Yu W, Hodges D H 2018. Mechanics of structure genome-based global buckling analysis of stiffened composite panels. Acta Mech: 1-16.

Molga M, Smutnicki C 2005. Test functions for optimization needs Test functions for optimization needs, 101.

Molina-Cristóbal A, Palmer P R, Skinner B A, et al. 2010 Multi-fidelity simulation modelling in optimization of a submarine propulsion system. 2010 IEEE Vehicle Power and Propulsion Conference. IEEE: 1-6.

Pires EJS, Machado JAT, de Moura OPB et al (2010) Particle swarm optimization with fractional-order velocity. Nonlinear Dyn 61(1-2):295–301

Quinn D, Murphy A, Glazebrook C (2012) Aerospace stiffened panel initial sizing with novel skin sub-stiffening features. Int J Struct Stab Dyn 12(05):1250060

Rouhi M, Ghayoor H, Hoa SV et al (2016) Stiffness tailoring of elliptical composite cylinders for axial buckling performance. Compos Struct 150:115–123

Shields MD, Zhang JX (2016) The generalization of Latin hypercube sampling. Reliab Eng Syst Saf 148:96–108

Sim CH, Park JS, Kim HI et al (2018a) Postbuckling analyses and derivations of knockdown factors for hybrid-grid stiffened cylinders. Aerosp Sci Technol 82:20–31

Sim CH, Kim HI, Lee YL et al (2018b) Derivations of knockdown factors for cylindrical structures considering different initial imperfection models and thickness ratios. Int J Aeronaut Space Sci 19(3):626–635

Song X G, Lv L Y, Sun W, et al. 2019 A radial basis function-based multi-fidelity surrogate model: exploring correlation between high-fidelity and low-fidelity models. Struct Multidiscip Optim: 1-17.

Sun FF, Fan HL, Zhou CW et al (2013) Equivalent analysis and failure prediction of quasi-isotropic composite sandwich cylinder with lattice core under uniaxial compression. Compos Struct 101:180–190

Tian K, Wang B, Zhang K et al (2018a) Tailoring the optimal load-carrying efficiency of hierarchical stiffened shells by competitive sampling. Thin-Walled Struct 133:216–225

Tian K, Wang B, Zhou Y, Waas AM (2018b) Proper-orthogonal-decomposition-based buckling analysis and optimization of hybrid fiber composite shells. AIAA J 56(5):1723–1730

Tian K, Wang B, Hao P, Waas AM (2018c) A high-fidelity approximate model for determining lower-bound buckling loads for stiffened shells. Int J Solids Struct 148:14–23

Tyan M, Nguyen NV, Lee JW (2015) Improving variable-fidelity modelling by exploring global design space and radial basis function networks for aerofoil design. Eng Optim 47(7):885–908

Viana F, Haftka R 2010. Surrogate-based optimization with parallel simulations using the probability of improvement. 13th AIAA/ISSMO Multidisciplinary Analysis Optimization Conference: 9392.

Vitali R, Haftka RT, Sankar BV (2002) Multi-fidelity design of stiffened composite panel with a crack. Struct Multidiscip Optim 23(5):347–356

Wang B, Hao P, Li G et al (2014) Optimum design of hierarchical stiffened shells for low imperfection sensitivity. Acta Mech Sin 30(3): 391–402

Wang B, Tian K, Hao P et al (2015) Hybrid analysis and optimization of hierarchical stiffened plates based on asymptotic homogenization method. Compos Struct 132:136–147

Wang B, Tian K, Zhou CH et al (2017a) Grid-pattern optimization framework of novel hierarchical stiffened shells allowing for imperfection sensitivity. Aerosp Sci Technol 62:114–121

Wang B, Tian K, Zhao HX et al (2017b) Multilevel optimization framework for hierarchical stiffened shells accelerated by adaptive equivalent strategy. Appl Compos Mater 24(3):575–592

Wang B, Du KF, Hao P et al (2019) Experimental validation of cylindrical shells under axial compression for improved knockdown factors. Int J Solids Struct 164:37–51

Wu H, Lai C, Sun F et al (2018) Carbon fiber reinforced hierarchical orthogrid stiffened cylinder: fabrication and testing. Acta Astronaut 145:268–274

Xu G (2013) An adaptive parameter tuning of particle swarm optimization algorithm. Appl Math Comput 219(9):4560–4569

Xu YM, Tong Y, Liu M et al (2016) A new effective smeared stiffener method for global buckling analysis of grid stiffened composite panels. Compos Struct 158:83–91

Zhao YN, Chen M, Yang F et al (2017) Optimal design of hierarchical grid-stiffened shells based on linear buckling and nonlinear collapse analyses. Thin-Walled Struct 119:315–323

Zhou Q, Shao X, Jiang P et al (2016a) An active learning metamodeling approach by sequentially exploiting difference information from variable-fidelity models. Adv Eng Inform 30(3):283–297

Zhou Q, Shao X, Jiang P et al (2016b) An active learning variable-fidelity metamodelling approach based on ensemble of metamodels and objective-oriented sequential sampling. J Eng Des 27(4-6):205–231